

# End-To-End Data-Dependent Routing in Multi-Path Neural Networks

Dumindu Tissera<sup>a,b</sup>, Kasun Vithanage<sup>b</sup>, Rukshan Wijesinghe<sup>a,b</sup>, Subha Fernando<sup>b</sup>, Ranga Rodrigo<sup>a,b</sup>

<sup>a</sup>Department of Electronic & Telecommunication Engineering, University of Moratuwa, Sri Lanka

<sup>b</sup>CodeGen QBITS Lab, University of Moratuwa, Sri Lanka

---

## Abstract

Neural networks are known to give better performance with increased depth due to their ability to learn more abstract features. Although the deepening of networks has been well established, there is still room for efficient feature extraction within a layer which would reduce the need for mere parameter increment. The conventional widening of networks by having more filters in each layer introduces a quadratic increment of parameters. Having multiple parallel convolutional/dense operations in each layer solves this problem, but without any context-dependent allocation of resources among these operations: the parallel computations tend to learn similar features making the widening process less effective. Therefore, we propose the use of multi-path neural networks with data-dependent resource allocation among parallel computations within layers, which also lets an input to be routed end-to-end through these parallel paths. To do this, we first introduce a *cross-prediction* based algorithm between parallel tensors of subsequent layers. Second, we further reduce the routing overhead by introducing feature-dependent *cross-connections* between parallel tensors of successive layers. Our multi-path networks show superior performance to existing widening and adaptive feature extraction, and even ensembles, and deeper networks at similar complexity in the image recognition task.

**Keywords:** Multi-path networks, Data-dependent routing, Image recognition

---

## 1. Introduction

It is a common practise to increase the depth of a deep neural network to gain more performance in a given task [9, 10, 19, 25, 29]. While the effective utilization of increasing the depth of a network is well established [9, 10, 19], the efficient utilization of resources in a given layer, i.e., rich feature extraction within layers, has not been explored well. Having many layers along the depth of a network which are separated by non-linear activations enables a network to approximate very complex distributions. While this is very important to learn in a complex dataset, it is also intuitive to have rich feature extraction processes in each layer, which would improve the utility of the network.

The naive way to have richer layer-wise feature extraction is to increase the number of convolutional filters or dense nodes in each layer [37]. This leads to a quadratic increase in the total number of parameters in terms of the width of the network, which is inefficient. As opposed to this conventional widening, it is

efficient to use multiple parallel operations in a given layer [29, 36], which limits the increment of parameters to be linear in terms of the width. Another approach, model ensembling [16, 25], feeds the same image to multiple independent neural networks and amalgamates each networks' response. Another class of work feeds different versions of the same image created by different pre-processing mechanisms to multiple independent networks [2, 33]. However, without a context-dependent resource allocation among the parallel computations, these widening processes tend to learn redundant information raising questions on the overall effectiveness of having parallel operations. In summary, the existing widening is not fully effective in terms of parallel resource utilization.

Consider a particular layer in a multi-path network which contains parallel sets of feature maps (paths). The architecturally parallel families of filters in each path learn independently. If homogeneous feature maps—those that concentrate on similar image features—are already grouped to parallel paths, each family of filters operating on each path can specialize the feature extraction to the particular context. Such a wise use of

---

This paper extends the work in Tissera *et al.* 2020 [31].

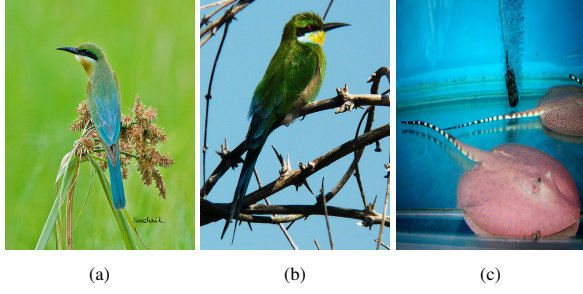


Figure 1: Intuition for sharing resources at multiple levels of layers: Three samples from the ILSVRC 2012 [22] validation set. The first two images show two hummingbirds, and the third image shows an electric ray. Image b and c share similar low-level features such as the dominant color, whereas, image a and b share similar abstract information such as body pose. Therefore, in initial layers of a multi-path network, processing image b and c feature maps together, and in deeper layers, processing image a and b feature maps together might yield better overall performance.

parallel resources increases the efficiency of feature extraction with respect to the number of filters used, as multiple small families of dedicated filters may extract a richer combination of features than a large single set of filters—or even multiple sequential filter sets (deepening). To do such grouping and to allocate incoming parallel tensors to these groups, we need a mechanism which routes between subsequent layers, i.e., to connect the parallel sets of feature maps (tensors) of a particular layer to the parallel paths in the next layer needing cross connections. This mechanism should further gate these connections according to the context of the previous layer’s tensors so that they get routed to the next layer adaptively. The parallel paths would be able to allocate resources efficiently with carefully designed routing.

It is also important to have such routing mechanisms throughout the depth of the multi-path network, preferably for each segment of layers, rather than allocating inputs to parallel paths at the very first layer and concatenating the outputs of the final layer. This is because the *context* of an image is captured throughout the depth of the neural network, each depth segment focusing at a different level of abstraction of the image. Therefore, in each layer, the homogeneous grouping of feature maps could be different from each other. We interpret an image’s context as a cumulative detail, which is not limited to the class. An image’s context, in the lowest level might represent the overall color, structure of edges etc. and, in deeper levels, more abstract information such as body pose or even the class. In addition, the real image context, which matters in the given task, might be

different from the human interpretation [14]. Therefore, routing captures context at different levels of abstraction distribute along the depth of the network.

Due to this reason, when a multi-path network with context-wise path allocation learns a particular task, images which get similar resource allocation in a particular depth might get a different allocation at another depth. For example, consider the three images from ILSVRC2012 [3] dataset shown in Figure 1. Image 1a shows a hummingbird sitting on a green bench where the background is grass. Image 1b is also a hummingbird but sitting on a thorny bench with the background as sky. Image 1c is an electric ray in water. If we consider a shallow layer (low-level) detail such as the overall color of the image, image 1b and 1c are similar to each other, whereas image 1a is different. However, if we consider an abstract detail such as the body pattern, image 1a and 1b are similar, and image 1c is different. Therefore, in initial layers of a multi-path network, image 1b and image 1c might get similar path allocations and in deeper layers, image 1a and 1b might get similar path allocations. To accommodate such different grouping according to the nature of features in each layer, we need routing mechanisms throughout the depth of a multi-path network.

In this paper, we introduce a novel layer-wise routing mechanisms to softly route an input image among the parallel paths in each layer of a multi-path network. The proposed data/feature-dependent routing algorithms delegates the data flow from the parallel sets of feature maps in a given layer to the parallel paths in the next layer. In detail, the main contributions of this paper are as follows,

- We first propose a cross-prediction based algorithm. Here, parallel tensors of a given layer predict each tensor in the next layer and gate (routing) probabilities of each of the incoming tensors. Each of the next layer’s parallel tensors is constructed by summing the predictions made by previous layer tensors weighted by the corresponding gate.
- We further propose a cross-connection based algorithm, where the previous layers tensors are directly weighted by computed gate probabilities and added together to construct the next layer of parallel tensors. This design reduces the routing overhead drastically while maintaining the performance.
- We show that the proposed multi-path networks exhibit superior performance to existing deepening,

widening and adaptive feature extraction methods. Further, we empirically justify the nature of context-dependent resource allocation and gate activation.

## 2. Related Work

Convolutional neural networks with many layers along the depth have proven to give excellent performance in the supervised learning domain [16, 25, 29], surpassing conventional shallow neural networks [17, 21]. However, having too many layers in a conventional neural network leads to performance degradation [9]. Residual Networks (ResNets) [9] mitigate this issue by using residual blocks which allow the gradients to flow to the initial layers with less attenuation through residual pathways. Identity mappings in residual networks [10] further clears the residual pathways enabling the training of very deep networks without gradient attenuation possible. However, these deepening approaches mainly focus on clearing the gradient flow pathways to efficiently train very deep networks, while it is also intuitive to improve the feature extraction process layer-wise.

The conventional width enhancement of convolutional neural networks by increasing the number of filters [37] or fully-connected nodes in each layer is inefficient as the added complexity outweighs the performance gain. Also, width increment results in quadratic parameter increment, which is inefficient. In contrast, ResNeXt [36] and Inception networks [28, 29, 30] use parallel operations in a given layer which limits the parameter increment to a linear scale. However, there is no context-dependent allocation of input feature maps among these parallel computations, hence, parallel paths tend to learn similar information. Model ensembling [16, 25], where multiple networks compute independent responses of the same input to compute the final output, is also subjected to this feature redundancy.

Instead of feeding the same input to multiple networks, it is more intuitive to feed different versions of the same input to parallel networks. Ciregan *et al.* 2012 [2] showed that having multi-column networks, where each set of columns is fed with inputs pre-processed in different ways, leads to improved performance. Wang 2015 [33] proposed a similar approach of using multi-path networks with different versions of input fed to different paths. However, these approaches do not connect parallel paths along with the depth, instead, these parallel columns tend to learn in isolation. Since each path is only focused on learning from a different version

of the same input, there is no context-dependent allocation of parallel resources. To have a multi-path network do such allocation layer-wise, we need connections between parallel computations throughout the depth of the network.

Cross-Stitch Networks [18] first introduced the cross-connections between parallel tensors in multi-path neural networks. The weighting coefficients of these cross-connections are learned independently as individual weights are static during inference. Sluice networks [20] and NDDR-CNN [5] further improve Cross-Stitch Networks. The purpose of these works is to determine the fixed mix of task-specific and shared resources in a parallel path network to perform multiple tasks for a single input (e.g., semantic segmentation and surface normal estimation). This is referred to as common multi-tasking [1] in the research community. To learn such a fixed mix of shared and task-specific pathways, having independently learned weighting of cross-connections is sufficient. In contrast, our intention of using parallel paths is to allocate incoming feature maps in each layer to parallel computations depending on their context, hence to route an input end-to-end to perform a certain task. Therefore, unlike in Cross-Stitch networks, in our case, the weighting of such connections should depend on the nature of the input.

Our work is closely related to existing adaptive feature extraction methods. We use the term adaptive feature extraction because in those methods, the main feature extraction process is supported by additional parametric or non-parametric functions. These functions are computed on the inputs to the network [8] or the inputs to each layer [11, 12, 13, 23, 26, 34, 32, 35]. This allows those networks to be flexible to the context of the input, making the network more dynamic during inference. Hypernetworks [8] include a smaller network embedded inside the main network to predict the weights of the main network. Squeeze-and-excitation networks (SENet) [13] introduce a learnable re-calibration of each convolutional channel, commonly known as channel-wise attention. Highway Networks [26, 27] propose the use of gates to learn to regulate the flow of information along the depth of the network to effectively train deep models. ConvNet-AIG [32] and BlockDrop [35] introduce a data-dependent selection criteria of residual blocks in a ResNet [9] according to the nature of the input. However, these approaches mostly utilize a common path for the main flow of information end-to-end, although the weights might vary. In contrast, our model has parallel paths with different weights in each path, enabling the model to vary the main flow of information through a selected combina-

---

**Algorithm 1** Cross-Prediction based routing between inputs and outputs of a routing layer.

---

**Input:**  $\mathbf{X} \{[\mathbf{X}_i \text{ for } i = 1, 2, \dots, m]\}$   
**Predictions from current layer:**  
  **for**  $i = 1$  **to**  $m$  **do**  
    **for**  $j = 1$  **to**  $n$  **do**  
       $\mathbf{U}_{ij} \leftarrow \mathbf{W}_{ij}\mathbf{X}_i + b_{ij}$   
    **end for**  
    **Gate Computation on  $\mathbf{X}_i$ :**  
       $\mathbf{Z}_i \leftarrow \text{global\_average\_pooling}(\mathbf{X}_i)$   
       $\mathbf{A}_i = [a_{i1}, \dots, a_{in}] \leftarrow \mathbf{W}_2^i(\text{ReLU}(\mathbf{W}_1^i \mathbf{Z}_i))$   
       $\mathbf{G}_i = [g_{i1}, \dots, g_{in}] \leftarrow \text{softmax}(\mathbf{A}_i)$   
    **end for**  
**Construction of outputs:**  
  **for**  $j = 1$  **to**  $n$  **do**  
     $\mathbf{Y}_j \leftarrow \text{ReLU}(\sum_{i=1}^n (g_{ij} \times \mathbf{U}_{ij}))$   
  **end for**  
**Output:**  $\mathbf{Y} \{[\mathbf{Y}_j \text{ for } j = 1, 2, \dots, n]\}$

---

tion of parallel resources in each layer according to the context facilitating context-dependent soft selection and sharing of resources. As a results, our network shows a significant performance gain and sheds more light on context-dependent routing of information.

### 3. Cross-Prediction Based Routing

To build end-to-end routing in a parallel path network, we should build a layer-wise routing mechanism to route between subsequent layers carrying parallel tensors in each. I.e., given a layer of parallel tensors, we need a mechanism to construct the next layer of parallel tensors. This mechanism should allow gated coupling between tensors in the two layers so that any tensor in the first layer can be routed to any tensor in the next layer. In our cross-prediction based algorithm, each tensor among parallel tensors in a particular layer performs convolutional or dense predictions for each of the tensors in the next layer. In addition, each tensor in the first layer also predicts the probabilities (denoted by gates) of that particular tensor being routed to each of the next layer tensors. The next layer of parallel tensors are constructed by taking the weighting the predictions by gates and adding together accordingly.

Suppose the inputs to a routing layer consist of  $m$  tensors  $[\mathbf{X}_{i=1, \dots, m}]$ , and the routing layer outputs  $n$  tensors  $[\mathbf{Y}_{j=1, \dots, n}]$ . First, each tensor in inputs performs predictions for each tensor in the outputs. The prediction  $\mathbf{U}_{ij}$ , which is made by tensor  $i$  in inputs ( $\mathbf{X}_i$ ) to tensor  $j$  in outputs ( $\mathbf{Y}_j$ ), is a linear, learnable transformation, which

can simply be shown as

$$\mathbf{U}_{ij} = \mathbf{W}_{ij}\mathbf{X}_i + b_{ij},$$

where  $\mathbf{W}_{ij}$  and  $b_{ij}$  correspond to weight and bias terms, respectively. If  $\mathbf{X}_i$  is a 3-dimensional tensor ( $\mathbf{X}_i \in \mathbb{R}^{W \times H \times C}$ ), this corresponds to a convolution.

In addition, each  $\mathbf{X}_i$  predicts an  $n$ -dimensional vector of gate values  $\mathbf{G}_i$ , which represents the  $n$  probabilities of  $\mathbf{X}_i$  being routed to each  $\mathbf{Y}_j$ , i.e.,  $\mathbf{G}_i$  can be expressed as  $[g_{i1}, \dots, g_{in}]$ , where,  $g_{ij}$  corresponds to the scalar gate value connecting  $\mathbf{X}_i$  to  $\mathbf{Y}_j$ .  $\mathbf{G}_i$  can be calculated by a non-linear parametric computation on  $\mathbf{X}_i$ , preferably two dense operations separated by *ReLU* activation. However, If  $\mathbf{X}_i$  is 3-dimensional, this occupies a significant amount of parameters. Therefore, if  $\mathbf{X}_i$  is 3-dimensional, to calculate  $\mathbf{G}_i$ , we first feed  $\mathbf{X}_i$  to a global average pooling operation, to produce  $1 \times 1 \times C$  latent channel descriptor  $\mathbf{Z}_i$  [13, 32]. Since each channel in a set of convolutional feature maps represents a particular feature of the input which is searched by a specific filter, global average pooling results in a compressed descriptor which still carries the information about the presence of each feature. Global average pooling further adds noise to the non-linear computation, which regularizes the gate computation. Each channel value  $(z_i)_c$  of the channel descriptor  $\mathbf{Z}_i$  can be obtained as,

$$(z_i)_c = \frac{1}{H \times W} \sum_{a=1}^H \sum_{b=1}^W (x_i)_{a,b,c}. \quad (1)$$

$\mathbf{Z}_i$  is then fed to a non-linear computation with two fully-connected layers comprised of 16 and  $n$  nodes respectively, separated by ReLU activation [6]. This operation yields  $n$  latent relevance scores  $\mathbf{A}_i$  ( $[a_{i1}, \dots, a_{in}]$ ) representing the relevance of the incoming tensor to the next layer tensors.

$$\mathbf{A}_i = \mathbf{W}_2(\text{ReLU}(\mathbf{W}_1 \mathbf{Z}_i)) \quad (2)$$

Finally, we impose softmax activation on top of the  $n$  relevance scores  $\mathbf{A}_i$  to calculate gate probabilities  $\mathbf{G}_i$ .

$$\mathbf{G}_i = \text{softmax}(\mathbf{A}_i), \text{ i.e., } g_{ij} = \frac{e^{a_{ij}}}{\sum_{k=1}^n e^{a_{ik}}}. \quad (3)$$

The activation  $\text{softmax}(\cdot)$  returns  $n$  scores, which represent the probabilities of  $\mathbf{X}_i$  being routed to each output  $\mathbf{Y}_{j=1, \dots, n}$ . Figure 3a shows the operations carried out by a 3-dimensional tensor at the input of a routing layer in the prediction phase.

Once the cross-predictions  $\mathbf{U}_{ij}$  and the gates  $\mathbf{G}_i$  are calculated, the outputs of the routing layer are calculated. To construct  $j^{\text{th}}$  output  $\mathbf{Y}_j$ , predictions made for

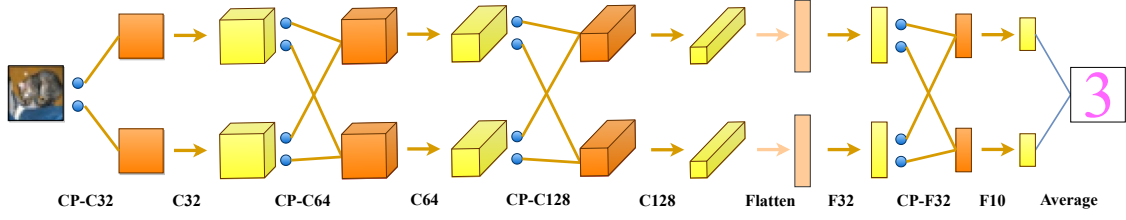


Figure 2: Two-path CNN with cross-prediction based routing (referred as BaseCNN-2-CP in the paper). CP- $Cn$  denotes a cross-prediction based routing layer where the cross predictions are convolutions with  $n$  filters. Similarly, CP- $Fn$  denotes a routing layer with dense cross-predictions of  $n$  nodes.  $Cn$  denotes a forward layer where parallel computations are convolutions each with  $n$  filters.  $Fn$  denotes a forward layer with parallel dense layers each containing  $n$  output nodes.

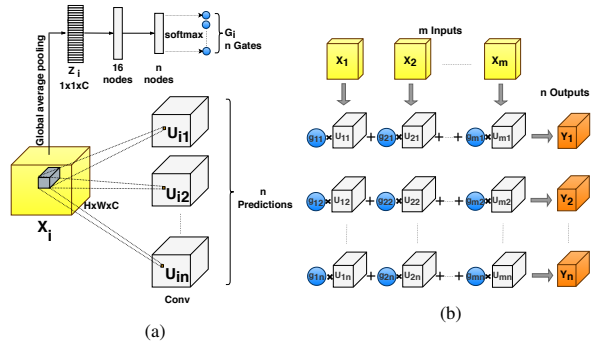


Figure 3: 3a: 3-dimensional tensor  $\mathbf{X}_i$  in inputs predicting  $n$  outputs of routing layer and associated gates. 3b: Constructing outputs of routing layer based on the predictions and gates computed by all such inputs  $\mathbf{X}_{i=1,\dots,m}$ . See Eq. 4.

$\mathbf{Y}_j$  ( $\mathbf{U}_{ij}$ ,  $i = 1, \dots, m$ ) are weighted by corresponding gate values ( $g_{ij}$ ,  $i = 1, \dots, m$ ) and added together. We further impose ReLU activation to the constructed tensor.

$$\mathbf{Y}_j = \text{ReLU} \left( \sum_{i=1}^n (g_{ij} \times \mathbf{U}_{ij}) \right) \quad (4)$$

This adaptive re-calibration of the predictions made by input tensors to construct the output tensors shares a similar intuition of attention introduced in SENets [13]. However, our intentions soft-routing information along different paths.

Figure 2 shows a two-path convolutional neural network with our routing added at selected locations which is referred to as BaseCNN-2-CP later. The routing process between two layers with  $m$  inputs and  $n$  outputs is illustrated in Figure 3. There, Figure 3a shows a particular tensor among the inputs to a routing layer predicting next layer tensors and its coupling probabilities to them. Figure 3b shows the construction of the outputs of the routing layer from the predictions and gates calculated by previous layer tensors. Algorithm 1 further explains

the routing between two layers.

We insert these routing layers in between selected layers in multipath networks (Figure 2), enabling other layers to have independent parallel paths to learn in an isolated manner. Adding one routing layer increases the effective depth of the network by one layer due to the cross-predictions being convolutional or dense operations. Since the output layer tensors are combinations of linear operations it is important to impose a non-linear *ReLU* activation before feeding the parallel tensors to next feed-forward computation. In the final layer, the parallel feature maps are averaged to produce a single output.

However, since each tensor in a given layer predicts each tensor in the subsequent layer in terms of a convolution or a dense operation, the number of parameters employed in the routing process between two layers is subjected to quadratic increment with the number of parallel paths. Having such an amount of routing overhead is not efficient. Therefore, to limit the routing overhead increment to be linear with the number of parallel paths, we introduce cross-connection based routing.

#### 4. Cross-Connection Based Routing

Cross-connection based routing is similar to the above explained cross-prediction based routing, instead it weights the input tensors of the routing layer to construct output tensors, rather than weighting cross-predictions that involve either dense or convolutional operations (describe in Sec. 3). This way, the quadratic increment of routing overhead with the number of parallel paths is overcome. The routing overhead now only contains the small number of parameters added from the non-linear gate computations. Also, a routing layer now becomes a mere cross-connecting layer and does not carry weights which are contributed to learning the main task. Therefore, inserting cross-connections

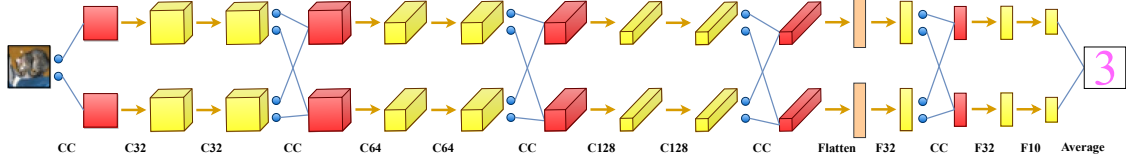


Figure 4: Two-path CNN with adaptive cross-connections inserted at selected locations (referred as BaseCNN-2-CC in the paper). CC denotes a cross-connecting layer where the gates and connections are shown by blue circles and edges, and the outputs of cross-connecting layer are shown in red boxes.  $C_n$  and  $F_n$  denotes forward convolutional and dense layers respectively, as in Fig. 2. The outputs of such forward layers are depicted by yellow boxes. Since the cross-connections are mere weighted connections, adding cross-connecting layers does not increase the effective depth of the network.

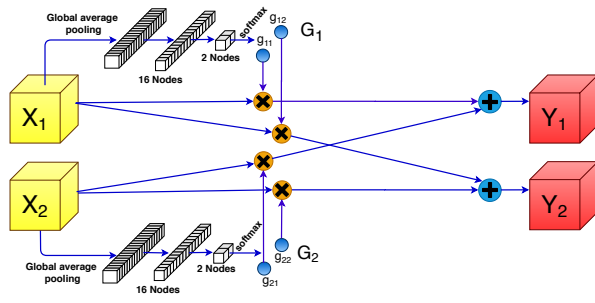


Figure 5: Cross-Connecting process between two layers, each with two parallel tensors. The gates which weigh the connections are computed from the input tensors by learnable parametric computations.

between layers in a multi-path network facilitates soft routing without the disadvantage of increasing the effective depth.

Given the  $m$  inputs  $[X_{i=1,\dots,m}]$ , to produce the  $n$  outputs  $[Y_{j=1,\dots,n}]$ , each  $X_i$  computes the gate vector  $G_i$  ( $[g_{i1}, \dots, g_{in}]$ ) as depicted by Eq. 1, Eq. 2 and Eq. 3. Given the gates, the algorithm next computes each  $Y_j$  output by summing the inputs  $[X_{i=1,\dots,m}]$  each weighted by the corresponding gate  $g_{ij,i=1,\dots,m}$ :

$$Y_j = \sum_{i=1}^m (g_{ij} \times X_i). \quad (5)$$

Since we directly connect inputs to construct outputs, the output tensor dimensions are same as the inputs. Figure 5 shows the cross-connecting process between two layers carrying two parallel tensors in each. Algorithm 2 illustrates the adaptive cross-connecting process.

The cross-connecting process can also be illustrated via matrix form to show the pixel-wise operations. Consider a set of 3-dimensional input tensors  $[X_{i=1,\dots,m}]$  and output tensors  $[Y_{j=1,\dots,n}]$ . Lets denote the pixel value at the location  $(a, b, c)$  of  $X_i$  as  $x_{ia,b,c}$ , and  $Y_j$  as  $y_{ja,b,c}$ .

**Algorithm 2** Cross-connection based routing between two adjacent layers with  $m$  input and  $n$  output sets of feature maps respectively.

**Input:**

$X$ : inputs  $\{[X_i \text{ for } i = 1, \dots, m]\}$

**Calculating gate values:**

**for**  $i = 1$  **to**  $m$  **do**

$Z_i \leftarrow \text{global\_average\_pooling}(X_i)$

$A_i = [a_{i1}, \dots, a_{in}] \leftarrow W_2^i(\text{ReLU}(W_1^i Z_i))$

$G_i = [g_{i1}, \dots, g_{in}] \leftarrow \text{softmax}(A_i)$

**end for**

**Construction of outputs:**

**for**  $j = 1$  **to**  $n$  **do**

$Y_j \leftarrow \sum_{i=1}^m (g_{ij} \times X_i)$

**end for**

**Return:**

$Y$ : outputs  $\{[Y_j \text{ for } j = 1, \dots, n]\}$

The set of output pixels at  $(a, b, c)$  are therefore,

$$\begin{bmatrix} y_{1a,b,c} \\ \vdots \\ y_{na,b,c} \end{bmatrix} = \begin{bmatrix} g_{11} & \cdots & g_{m1} \\ \vdots & \ddots & \vdots \\ g_{1n} & \cdots & g_{mn} \end{bmatrix} \begin{bmatrix} x_{1a,b,c} \\ \vdots \\ x_{ma,b,c} \end{bmatrix}. \quad (6)$$

This formulation is similar to Cross-Stitch Networks [18]. However, their coupling coefficients  $g_{ij}$  are independently trained weights. This only allows learning the mix of shared and task-specific representations to perform multiple tasks on a single input which is fixed during inference. In our algorithm,  $g_{ij}$ s are produced by a parametric computation on inputs  $X_i$  themselves, using the channel-wise attention mechanism [13]. This allows to dynamically change the mix of context-specific and shared representations according to the nature of the diverse input, to perform a given task.

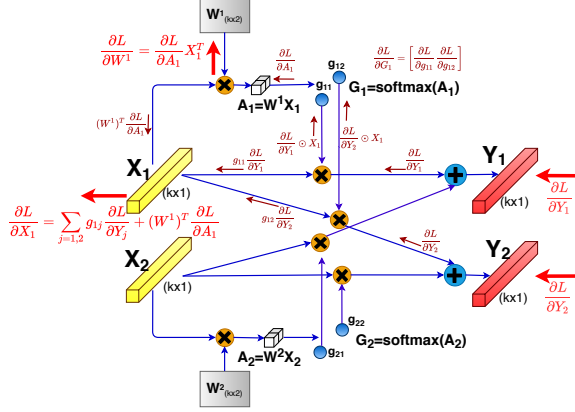


Figure 6: The simplified cross-connecting process between two subsequent layers carrying two parallel tensors in each. Gradient flows to the top tensor in the input layer  $X_1$  and its gate computation weight matrix  $W^1$  are shown.

## 5. Back-propagating Errors through Cross-Connections

We saw in Sec. 4 that cross connection facilitates soft-routing in a context-specific manner. Training a network with cross connections need backpropagation of errors through them. The backpropagation through a cross-connecting layer, represented by Eq. 5 and 6, is not straight forward as in Cross-Stitch networks [18] where the coupling coefficient matrix consists of independently learned weights. In this case, the elements in the gating matrix  $\mathbf{G}$  are constructed from the input  $\mathbf{X}$  itself. Therefore the gradients flown to each input  $\mathbf{X}_i$  consists not only the direct gradient weighted by gate element, but also another component from the gate computation. Also, instead of directly optimizing gates, the weights which produce the gates are getting optimized.

For the simplicity of explanation, let's assume that the tensors  $\mathbf{X}$  and  $\mathbf{Y}$  are  $k$ -dimensional vectors, and the gate calculation only has a simple fully-connected layer as opposed to Eq. 1 and Eq. 2. Figure 6 shows this simplified cross-connecting operation for two-parallel paths. With this simplified operation, calculation of the relevance scores  $\mathbf{A}_i$  from each  $\mathbf{X}_i$  reduces to,

$$\mathbf{A}_i = \mathbf{W}^i \mathbf{X}_i, \quad (7)$$

where  $\mathbf{W}^i$  is a  $n \times k$  matrix of weights.  $\mathbf{G}_i$  is computed by taking *softmax* of these logits as usual (Eq. 3). Then, output tensors  $\mathbf{Y}_{j(j=1\dots n)}$  are constructed as in Eq. 5. Here, our goal is to find gradients w.r.t each  $\mathbf{X}_{i(i=1\dots m)}$  and  $\mathbf{W}_{(i=1\dots m)}^i$ , given the gradients of loss w.r.t. each output  $\mathbf{Y}_{j(j=1\dots n)}$ . I.e., given  $\frac{\partial L}{\partial \mathbf{Y}_j}$ , to compute  $\frac{\partial L}{\partial \mathbf{W}^i}$

and  $\frac{\partial L}{\partial \mathbf{X}_i}$ . Figure 6 shows the flow of gradients to  $\mathbf{W}^1$  and  $\mathbf{X}_1$  from  $\mathbf{Y}_{j(j=1,2)}$  in a 2 parallel path cross-connecting operation, which aids understanding the detailed flow of errors explained below.

It is important to propagate the incoming error to each  $g_{ij}$  first. The scalar  $g_{ij}$  is used to multiply each element of  $\mathbf{X}_i$  when producing  $\mathbf{Y}_j$  (Eq. 5). Therefore, the partial derivative of loss w.r.t.  $g_{ij}$  is the summation of the element-wise multiplication between the gradient vector and  $\mathbf{X}_i$ ,

$$\frac{\partial L}{\partial g_{ij}} = \sum_k \frac{\partial L}{\partial \mathbf{Y}_j} \odot \mathbf{X}_i.$$

With all such  $\frac{\partial L}{\partial g_{ij}}$ , we can form  $\frac{\partial L}{\partial \mathbf{G}_i}$  as an  $n$ -dimensional column vector,

$$\frac{\partial L}{\partial \mathbf{G}_i} = \begin{bmatrix} \frac{\partial L}{\partial g_{i1}} & \dots & \frac{\partial L}{\partial g_{in}} \end{bmatrix}^T.$$

Propagating error to the relevance scores  $\mathbf{A}_i$  involves multiplying the gradients w.r.t  $\mathbf{G}_i$  by the partial derivative of gate values w.r.t the relevance scores  $\frac{\partial \mathbf{G}_i}{\partial \mathbf{A}_i}$ , i.e.,

$$\frac{\partial L}{\partial \mathbf{A}_i} = \frac{\partial \mathbf{G}_i^T}{\partial \mathbf{A}_i} \frac{\partial L}{\partial \mathbf{G}_i} = (\mathbf{J}_{\mathbf{A}_i}^{\mathbf{G}_i})^T \frac{\partial L}{\partial \mathbf{G}_i}.$$

Here,  $\mathbf{J}_{\mathbf{A}_i}^{\mathbf{G}_i}$  is the Jacobian matrix of the derivative of softmax approximation,

$$\frac{\partial \mathbf{G}_i}{\partial \mathbf{A}_i} = \mathbf{J}_{\mathbf{A}_i}^{\mathbf{G}_i} = \begin{bmatrix} g_{i1}(1 - g_{i1}) & \dots & -g_{i1}g_{in} \\ \vdots & \ddots & \vdots \\ -g_{in}g_{i1} & \dots & g_{in}(1 - g_{in}) \end{bmatrix}.$$

The gradients of loss w.r.t.  $\mathbf{W}^i$  can now be obtained by propagating the gradient w.r.t  $\mathbf{A}_i$  through Eq. 7. Therefore,

$$\frac{\partial L}{\partial \mathbf{W}^i} = \frac{\partial L}{\partial \mathbf{A}_i} \mathbf{X}_i^T = (\mathbf{J}_{\mathbf{A}_i}^{\mathbf{G}_i})^T \frac{\partial L}{\partial \mathbf{G}_i} \mathbf{X}_i^T. \quad (8)$$

It is also important to calculate the gradient of loss w.r.t  $\mathbf{X}_i$ , since this is the gradient which is propagated to the layer below.

$$\begin{aligned} \frac{\partial L}{\partial \mathbf{X}_i} &= \sum_{j=1}^n g_{ij} \frac{\partial L}{\partial \mathbf{Y}_j} + (\mathbf{W}^i)^T \frac{\partial L}{\partial \mathbf{A}_i} \\ &= \sum_{j=1}^n g_{ij} \frac{\partial L}{\partial \mathbf{Y}_j} + (\mathbf{W}^i)^T (\mathbf{J}_{\mathbf{A}_i}^{\mathbf{G}_i})^T \frac{\partial L}{\partial \mathbf{G}_i} \end{aligned} \quad (9)$$

Here, the first part of the loss is the direct flow of error to  $\mathbf{X}_i$  from the multiplication operation between  $g_{ij}$  and  $\mathbf{X}_i$ . The second term reflects the portion of the error propagated to  $g_{ij}$  from that particular multiplication flowing back to  $\mathbf{X}_i$ . This residual error is due to the attention-like gating mechanism which produces  $g_{ij}$  from  $\mathbf{X}_i$  itself.



Table 1: Notations and details of the compared convolutional neural networks:  $Cn$  denotes a convolutional layer of  $n$  filters.  $Fn$  denotes a fully connected layer of  $n$  output nodes.

Network	Structure
BaseCNN	$C32\ C32\ C64\ C64\ C128\ C128\ F32\ F32\ F10$
WideCNN	$C64\ C64\ C128\ C128\ C256\ C256\ F32\ F32\ F10$
DeepCNN	$C32\ C32\ C64\ C64\ C128\ C128\ C128\ C128\ C256\ C256\ C256\ F32\ F32\ F10$
BaseCNN-X	BaseCNN-X paths. No routing.
Base Ensemble	Ensemble of 3 BaseCNNs
All Ensemble	Ensemble of BaseCNN, WideCNN and DeepCNN
SEBaseCNN	SENet ([13]) on BaseCNN
SEDeepCNN	SENet ([13]) on DeepCNN
Cr-Stitch2	Cross-stitch network ([18]) with 2 parallel BaseCNNs
BaseCNN-X-CP	BaseCNN-X paths-cross-prediction based routing
BaseCNN-X-CC	BaseCNN-X paths-cross-connections

## 6. Image Recognition Performance

We conduct various experiments in the image-recognition task, to validate the effectiveness of having parallel paths with data-dependent resource allocation. We first evaluate the impact of having parallel paths in conventional convolutional neural networks. Then, we build custom Residual Networks (ResNets) [9] with parallel paths and our routing algorithms. In both cases, we compare our multi-path networks with wide networks, existing adaptive feature extracting methods and deeper networks of similar-complexity. Among the existing related methods, if the performance of models which carry similar complexity to our multi-path networks are not reported, we build custom models which match the complexity to our models.

### 6.1. Conventional Convolutional Neural Networks with Parallel Paths

In this section, we add parallel paths to conventional convolutional neural networks and compare with conventional network widening, deepening and other related networks. Table 1 shows the details of the networks we use for this purpose. We choose a 9 layer convolutional neural networks (6 convolutional layers and 3 dense layers) as the baseline, denoted as BaseCNN. We build our multi-path networks based on the BaseCNN.

BaseCNN-X-CP denotes an X-path network with cross-prediction based routing, where each path is similar to a BaseCNN. Figure 2 shows BaseCNN-2-CP architecture which uses two parallel paths. Here,  $1^{st}$ ,  $3^{rd}$  and  $5^{th}$  convolutional layers, and  $2^{nd}$  dense layer are replaced by cross-prediction based routing layers. Since cross-predictions are convolutions or dense operations,

one routing layer adds one layer to the effective depth of the network. Therefore we replace the selected layers in parallel path BaseCNN with the routing layers to maintain the same depth as BaseCNN. The outputs of the last layer of parallel dense operations are averaged to produce the final prediction.

BaseCNN-X-CC is an X-path network with adaptive cross-connections. Figure 4 shows BaseCNN-2-CC architecture which has two parallel paths. We insert a one-to-many connector to expand the input image to parallel paths and add cross-connections after the  $2^{nd}$ ,  $4^{th}$  and  $6^{th}$  convolutions and after the  $1^{st}$  dense layer. Since a cross-connection based routing layer contains only cross-connections and weighting coefficients, adding such layer does not increase the effective depth of the network. Therefore we insert these layers to the BaseCNN multi-path network without replacing any forward layers.

We double the filter size in each convolution to widen the BaseCNN, resulting in WideCNN. We also add more convolutional layers to the BaseCNN, which results in the DeepCNN architecture. To compare with an equivalent multi-path network which does not have intermediate routing, we build BaseCNN-X where X stands for the number of parallel BaseCNNs sharing the same input and the output (Averaging). To compare with model ensembles, we use an ensemble of 3 BaseCNNs which are trained individually (Base Ensemble). The output of the Base Ensemble is computed by averaging the individual BaseCNN responses at inference. We also build an ensemble of BaseCNN, WideCNN and DeepCNN, which is referred to as All Ensemble. To compare our multi-path networks with equivalent SENets [13], we add SE operations in convolutional layers of BaseCNN and DeepCNN, which results in SEBaseCNN and SEDeepCNN respectively. We replace the adaptive cross-connections in BaseCNN-2 with cross-stitching operations to build an equivalent two-path Cross-Stitch Network, Cr-Stitch2.

First, we train these models in the CIFAR10 dataset [15] for 200 epochs with a batch size of 128. We use Stochastic Gradient Descent (SGD) with a momentum of 0.9 and an initial learning rate of 0.1, which is decayed by a factor of 10 after 80 and 150 epochs. We augment the input images by random pixel shift in both directions, which is subjected to a maximum shift of 4 pixels, and random horizontal flipping. Table 2 shows the results of this study. For each model, we report the best performance out of 3 trials.

Adding parallel paths to BaseCNN with our routing algorithms improves the performance of BaseCNN, and also surpasses conventional widening. In this partic-



Table 2: Ablation study of CNNs in CIFAR10 - Classification errors (%). BaseCNNs with parallel paths and routing, at similar or less complexity, show superior performance compared to conventional widening, model ensembles, SENets, Cross-stitch networks and even conventional deepening. Considering the number of parameters utilized, adaptive cross-connections show the best performance. All networks are trained for 200 epochs. We further report our multi-path network performance after training for 350 epochs to set the benchmark (Column Error%<sup>†</sup>). Among the compared networks, \* denotes performance stated in the respective paper.

Network	Params (M)	Error%	Error% <sup>†</sup>
BaseCNN	0.55	9.26	
WideCNN	1.67	8.96	
DeepCNN	2.0	8.49	
BaseCNN-3	1.5	9.41	
BaseCNN Ensemble	1.66	7.87	
All Ensemble	4.27	6.9	
SEBaseCNN	0.58	8.99	
SEDeepCNN	2.06	8.15	
Cr-Stitch2	1.11	7.89	
VGG16 ([25])	14.9	6.98	
Sabour <i>et al.</i> [23]	8.2	10.6	
Highway* ([26, 27])	2.3	7.54	
<b>BaseCNN-2-CP</b>	1.3	7.24	<b>6.48</b>
<b>BaseCNN-3-CP</b>	2.23	<b>6.63</b>	<b>6.04</b>
<b>BaseCNN-4-CP</b>	3.34	<b>6.45</b>	<b>5.91</b>
<b>BaseCNN-2-CC</b>	1.11	7.03	<b>6.53</b>
<b>BaseCNN-3-CC</b>	1.67	<b>6.51</b>	<b>6.09</b>
<b>BaseCNN-4-CC</b>	2.22	<b>6.55</b>	<b>6.26</b>

ular setting, BaseCNN with two paths and our routing (BaseCNN-2-CP/CC) is sufficient to surpass the WideCNN, which has two times filters in each layer. Due to the quadratic increment of parameters with conventional widening, WideCNN carries nearly four times parameters of BaseCNN whereas having two parallel paths only doubles the number of parameters. Even with the routing overhead added, the total number of parameters of BaseCNN-2-CP is still significantly less than WideCNN, where BaseCNN-2-CC carries almost same amount of parameters as two BaseCNNs due to cross-connection based routing adding a very little amount of routing overhead.

BaseCNN-3-CP and -CC, with a clear margin, show superior performance to BaseCNN-3, which does not have intermediate routing. Also, BaseCNN-3-CP and -CC outperform the ensemble of 3 BaseCNNs, and even the ensemble of BaseCNN, WideCNN and DeepCNN. This indicates that the improvement of our multi-path networks is not merely due to the widened nature, but also due to the adaptive routing mechanisms. In this ex-

periment, BaseCNN-2-CP/CC even surpasses the DeepCNN, whose total number of parameters is more than three times the parameters in the BaseCNN. Finally, our multi-path nets even surpass the VGG16 [25] which consumes a large number of parameters along with both depth and width.

BaseCNN-2-CP/CC surpasses the cross-stitch network (Cr-Stitch2) with two paths, proving that adaptive cross-routing is more suitable to learn a task while handling the diversity rather than independently learned cross-stitching coefficients. BaseCNN-2-CP/CC further surpasses the SE Nets built based on the WideCNN and DeepCNN, showing the effectiveness of utilizing parallel paths over re-calibration of a single path. Among the other methods for rich layer-wise feature extraction or adaptive feature extraction, ours surpass Highway networks [26], and Capsule Networks [23] at similar or less complexity.

To learn from CIFAR10, adding a parallel path to BaseCNN (BaseCNN-2-CP/CC) gives a significant performance improvement. However, the performance gain is not that significant with the addition of the third parallel path (BaseCNN-3-CP/CC). The addition of the fourth path (BaseCNN-4-CP/CC) gives little or no improvement. Therefore, it is important to carefully design the number of parallel paths according to the dataset to get the best performance for the number of parameters utilized. However, this phenomena is common to all deepening [9, 10] and widening [37, 36] techniques.

The multi-path networks with cross-connections (BaseCNN-X-CC) use significantly less amount of parameters compared to the networks with cross-prediction based routing (BaseCNN-X-CP), which is more evident with the increased number of parallel paths. This is because adaptive cross-connections drastically reduce the routing overhead by eliminating the cross-convolutions or cross-dense operations in cross-prediction based routing. Cross-connection based routing also gives a similar performance to cross-prediction based routing, yielding better performance with respect to the model complexity. We further set the benchmark for CNN based multi-path networks: We re-train our multi-path nets in the previous setting but for 350 epochs, where the learning rate is decayed after 150 and 250 epochs respectively. The benchmark values are shown in the final column of Table 2.

## 6.2. Residual Networks with Parallel Paths

Next, we extend the residual networks (ResNets) [9] with parallel paths and our routing schemes. First, we add parallel paths to the ResNet variants which are designed to learn from small-scale datasets (ResNet20,

Table 3: Comparison of ResNets. ResNet20-3 outperforms ResNet110. ResNet20-3/4 and ResNet32-3/4 show on-par or superior performance to existing adaptive architectures which are mostly based on ResNet110. BaseCNN-X architectures surpass CNN based adaptive image classifiers which have similar or more number of parameters.

Network	Params (M)	CIFAR10	CIFAR100
ResNet20 [9]	0.27	8.75	-
ResNet110	1.7	6.61	26.88
ResNet164	2.5	5.93	25.16
WRN-40-2 [37]	2.2	5.33	26.04
HyperWRN40-2 [7]	0.15	7.23	-
SEResNet110 [13]	1.7	5.21	<b>23.85</b>
BlockDrop [35]	1.7	6.4	26.3
ConvNet-AIG [32]	1.78	5.76	-
ConvNet-AIG all [32]	1.78	5.14	-
<b>ResNet20-2-CP</b>	0.59	5.86	27.7
<b>ResNet20-3-CP</b>	0.92	<b>4.99</b>	<b>25.13</b>
<b>ResNet20-4-CP</b>	1.29	<b>4.81</b>	<b>23.82</b>
<b>ResNet20-2-CC</b>	0.55	5.5	27.36
<b>ResNet20-3-CC</b>	0.82	5.18	25.76
<b>ResNet20-4-CC</b>	1.1	<b>4.96</b>	<b>24.81</b>
<b>ResNet32-2-CC</b>	0.94	5.14	25.96
<b>ResNet32-3-CC</b>	1.41	<b>4.96</b>	<b>24.51</b>
<b>ResNet32-4-CC</b>	1.88	<b>4.59</b>	<b>23.52</b>

ResNet32 etc.). In these models, an initial convolution is followed by 3 sequential stacks, where, in each stack, several residual blocks (In ResNet20, 3 residual blocks in each stack) are employed. Each stack starts with a stridden residual block, resulting in down-sampled feature maps. The network terminates with a global average pooling layer, followed by the final dense layer which outputs the class probabilities.

To build parallel path ResNets with cross-prediction based routing (ResNet-X-CP), we replace the initial convolutional layer with a convolutional one-to-many routing layer and add two more routing layers before  $2^{nd}$  and  $3^{rd}$  stacks respectively. The parallel dense layer outputs are averaged to produce the final output. This design adds two more layers to the effective depth. To build parallel path ResNets with cross-connection based routing (ResNet-X-CC), we add one-to-many router after the initial convolution, and add three more cross-connection based routers after  $1^{st}$ ,  $2^{nd}$  and  $3^{rd}$  stacks respectively. Since these cross-connections do not contain convolutions, this design preserves the original depth of the network.

To train our models in CIFAR10 and CIFAR100 [15]

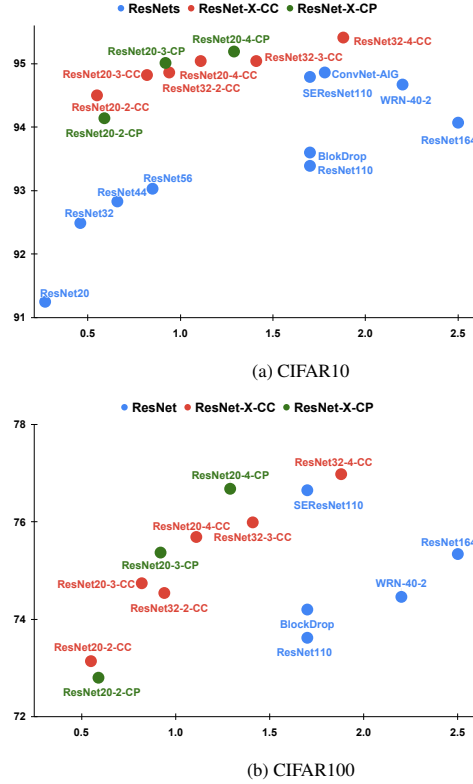


Figure 7: ResNet performance (accuracy) in CIFAR10 and CIFAR100 along with the number of parameters in millions. Blue circles correspond to conventional ResNets and ResNet based adaptive networks. Green circles show multi-path ResNets with cross-prediction based routing. Red circles show multi-path ResNets with cross-connection based routing. Our multi-path networks yield the best performance w.r.t the network complexity. Our networks (red and green) flocking to the top-left show that they show superior performance with less number of parameters, in general.

datasets, we use a similar setting to the previous study. We use a batch-size of 64, and train our models for 350 epochs where the learning rate is decayed after 150 and 250 epochs. For each model, we conduct three trials and report the best performance. Table 3 shows the recorded classification errors of our models and the reported errors of conventional ResNets and ResNet based adaptive feature extractors.

ResNet20 with three paths and our routing algorithms (ResNet20-3-CP/CC) surpasses the performance of the WideResNet40-2 (WRN-40-2), which has a depth of 40 layers and two times filters in each convolutional layer. The Hyper Network [8] built on top of WideResNet-40-2 (HyperWRN40-2) shows an inferior performance to the original WRN-40-2 although it uses a few numbers of parameters. In CIFAR10, ResNet20 with two paths

surpass ResNet110 and in CIFAR100, ResNet20 with three parallel paths surpasses ResNet110. This is impressive, as compared to ResNet110, ResNet20 is very shallow, and even with parallel paths added (2/3/4) the total number of parameters is still less than ResNet110.

Further, ResNet based multi-path networks surpass existing adaptive feature extraction methods, which are built on ResNet110. The BlockDrop [35] architecture, which is built on ResNet110, shows inferior performance to all our multi-path networks in CIFAR10 and shows better performance to only ResNet20-2-CP/CC in CIFAR100. ResNet20-3/4-CP, ResNet20-4-CC, and ResNet32-3/4-CC show superior performance to the ConvNet-AIG [32], which is based on ResNet110. All our multi-path networks except ResNet20-2-CC/CP surpass the SENet [13], which is built using ResNet110 with identity mappings [10] in CIFAR10. In CIFAR100, ResNet20-4-CP shows on-par performance to SEResNet110, and ResNet32-4-CC surpasses its performance. Among our multi-path nets, all the networks other than ResNet32-4-CC have less number of parameters than ResNet110 based networks.

Figure 7 plots the accuracies of the compared networks in CIFAR along with the number of parameters utilized. These plots clearly illustrate that our multi-path networks show the best utility of the network for the used number of parameters. Multi-path ResNets with cross-prediction based routing gives the best performance for a given depth. However, we prefer cross-connection based multi-path ResNets due to the less complex routing algorithm, which adds significant less routing overhead to the widening.

### 6.3. Multi-path ResNets on ILSVRC2012

Here, we further evaluate our multi-path ResNets in the ILSVRC 2012 Dataset [3, 22]. This image recognition dataset contains 1.3M training images and 50k validation images which are distributed under 1000 categories. To train in this dataset, we expand the residual networks which are originally designed to learn in the ImageNet dataset [9] with parallel paths. These residual networks share a similar setting to the thin residual networks which are designed to learn from CIFAR. These have an initial 7×7 convolution with a stride of 2 followed by a max-pooling operation. Thereafter, four sequential stacks of residual blocks are employed where each stack contains a pre-defined number of residual blocks sharing the same feature map size. Each stack’s first residual operation starts with a stridden convolution which downsamples the feature maps by a factor of 2. The final residual block’s response is fed to a global

Table 4: Single-crop and 10-crop validation error (%) in ILSVRC2012 dataset. ResNet18-2 with two paths comfortably outperforms ResNet18 and show on-par performance to ResNet34. It also surpasses the WideResNet18, which has 1.5 times filters in each layer. In the subset of ILSVRC2012, which contains the first 100 classes, ResNet50-2-CC, with similar or fewer model parameters, outperforms WideResNet and ResNext counterparts, and even twice deep ResNet101. \* denotes reproduced results

Network	Params	Single-Crop		10-Crop	
		Top-1	Top-5	Top-1	Top-5
Full Dataset					
ResNet18 [4, 37]	11.7M	30.4	10.93	28.22	9.42
ResNet34 [9, 37]	21.8M	26.77	8.77	24.52	7.46
WRN-18-1.5 [37]	25.9M	27.06	9.0		
<b>ResNet18-2-CC</b>	23.4M	<b>26.48</b>	<b>8.6</b>	<b>24.5</b>	<b>7.34</b>
Subset of first 100 classes					
ResNet50*	23.71M	20.46	4.96	19.26	4.72
ResNet101*	42.7M	19.16	4.58	17.78	4.44
WideResNet50-2* [37]	62.0M	19.82	5.02	18.62	4.76
ResNeXt50-2-64* [36]	47.5M	20.26	5.06	19.0	4.84
<b>ResNet50-2-CC</b>	47.5M	<b>18.64</b>	<b>4.34</b>	<b>17.62</b>	<b>4.0</b>

average pooling operation and the final fully connected layer which outputs the class response.

Since the cross-connection based routing is less complex, uses a very little overhead and still gives reasonably similar results to cross-prediction based routing, we only use cross-connection based routing in expanding these models to parallel paths. In particular, after the initial convolution and max-pooling, we insert a one-to-many adaptive router, which expands the network to parallel paths and insert cross-connection based routing layers after each stack containing residual blocks of certain feature map size. Finally, we average the final layer parallel dense predictions.

We expand ResNet18 with two parallel paths and cross-connection based routing (ResNet18-2-CC) and train in the dataset for 120 epochs with a batch size of 256, on two GPUs. We use SGD optimizer with the momentum of 0.9 and an initial learning rate of 0.1, which is decayed by a factor of 10 after every 30 epochs. We use standard data augmentation of re-scaling to 256×256, taking random crops of 224×224, and randomly flipping in the horizontal axis. To further evaluate deeper models with parallel paths, we use a subset of the ILSVRC dataset, which contains the first 100 classes only. This subset contains 130k training images and 5k validation images. To learn in this subset, we expand ResNet50 with two paths and cross-

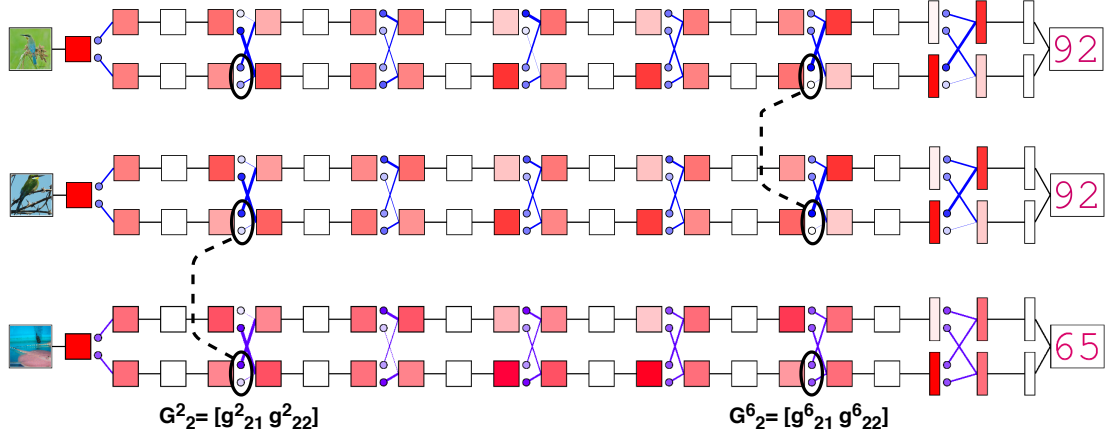


Figure 8: Route visualizations through cross-connections of VGG13-2 for the three images in Fig. 1. In each cross-connecting layer, the relative strengths of input and output tensors are shown in red intensities and the gate strengths are shown in blue intensities and connection thicknesses. Gating vector  $G^2_2$  shows similar gating patterns for image 1b and image 1c where gating vector  $G^6_2$  shows similar gating patterns for image 1a and image 1b. Observe the context-based resource allocation that varies along with the depth.

connection based routing (ResNet50-2-CC). We use a similar training setup as in the full dataset, except that the models are trained for 90 epochs. To compare with ResNet50-2-CC in this subset, we train ResNet50 and WideResNet50-2, which has two times filters in each layer and ResNeXt50-2-64, which has two parallel operations in each layer and ResNet101.

Table 4 shows the results of this study. ResNet18 with two parallel paths and cross-connections, in the ILSVRC 2012, comfortably surpass the performance of the single path ResNet18 and shows on-par performance to ResNet34. It also surpasses the performance of WideResNet18 with 1.5 times convolutional filters in each layer which still has more parameters than ResNet18-2-CC. In the subset, ResNet50-2-CC surpasses its single path baseline (ResNet50) and both WideResNet50-2 and ResNeXt50-2-64 confirming the superiority of our approach to existing widening at similar complexity. ResNet50-2-CC even shows slightly better results to the ResNet101, which is twice deep.

Overall, these experiments validate that our multi-path networks along with the adaptive routing algorithms show efficient usage of the resources in each layer. Due to this efficient use of layer resources, our multi-path networks, at similar or less complexity, show superior performance to conventional widening and other methods for rich layer-wise feature extraction, and even conventional deepening.

## 7. Visualization of Multi-path Learning

In this section, we use several visualization techniques to study the gating patterns of the cross-connection based routing scheme. For this purpose, we use a VGG13 [25] network with half the filters (32, 64, 128, 256) in each convolutional layer and 256 nodes in each dense layer. We join two such networks through cross-connections, where the routing layers are added after each pooling operation and after the first dense layer, following a similar pattern to the multi-path networks in Section 4). We train this network in a subset of the ILSVRC2012 which contains the first 100 classes.

First, we visualize the routing patterns of this trained network and show the differences in gating patterns, observed in layers at varying depths of the network. To further understand these gating patterns, we maximize a set of selected gating neurons and plot the network for images from the validation datasets that activate the neurons most and further synthesize randomly initialized images to maximize gating neurons. Also, we plot the gate activations of selected classes to understand the class-wise gate activation. Finally, we plot weight histograms of the two parallel paths at selected layers, to demonstrate that each path is capable of learning distinct information.

### 7.1. Visualization of Routing

We visualize the routing flow through cross-connections of the trained 2-path network to understand the gating patterns. Figure 8 shows such visualizations for the three images depicted in Figure 1. For each

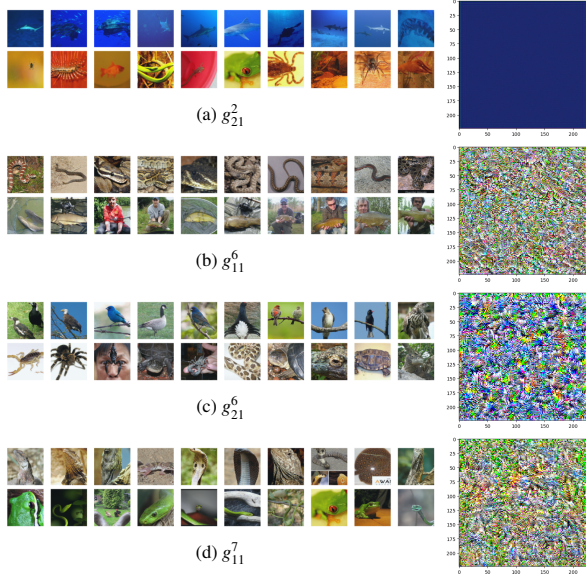


Figure 9: Maximization of selected gates: Each subfigure, corresponding to a particular gate, shows the 10 images with the highest gate activation (top left), the 10 images with the lowest gate activation (bottom left) and the synthesized image such that the gate neuron is maximized.  $g_{21}^2$  which is within initial layers is maximized for blue while the other gates which lie within deeper layers get triggered for more abstract features such as snake body patterns ( $g_{11}^6$ ), bird patterns ( $g_{21}^6$ ) and raised upper body patterns ( $g_{11}^7$ ).

cross-connection based routing layer which has two parallel inputs, two parallel outputs and gates which weigh the connections, we plot the relative activation strengths of input and output tensors and the gate strengths. We calculate the relative activation strength of a tensor by taking the average activation value of that tensor and normalizing by all such values of the parallel tensors of that layer. We map these relative activation strengths to red intensities and use these colours to colour each box representing the particular tensor. The softmax gate values computed by each input are directly mapped to blue intensities and thickness values which are then used to colour the circles denoting each gate and edges denoting each weighted connection respectively. We denote the stacks of conventional forward layers by uncoloured boxes. They contain sequential convolutions or dense operations which run in parallel, but no cross-operations are performed.

Let  $G_i^l$  ( $[g_{i1}^l, g_{i2}^l]$ ) be the gating vector computed by the  $i^{th}$  input tensor to the  $l^{th}$  cross-connecting layer. In these routing plots, we pay attention to the gating vectors  $G_2^2$  ( $[g_{21}^2, g_{22}^2]$ ) and  $G_2^6$  ( $[g_{21}^6, g_{22}^6]$ ) in particular.  $G_2^2$ , lying within initial layers of the network, show similar

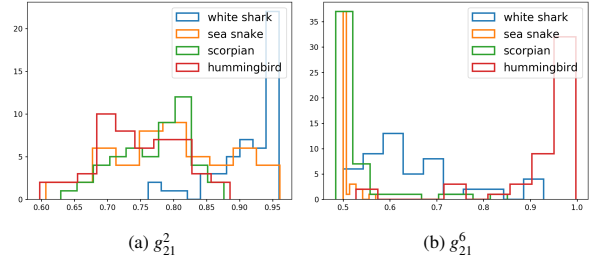


Figure 10: Gate activation histograms for chosen four classes in ILSVRC 2012 validation set. White shark, with mostly blue seawater as the background, has overall high activation for  $g_{21}^2$  while other classes are evenly distributed. Hummingbird images mostly activate  $g_{21}^6$  while other classes, agreeing less with bird patterns show less  $g_{21}^6$  activation. If the triggering pattern of any gate is commonly found in a certain class, those class members get similar gating in that layer.

gating patterns to image 1b and image 1c (maximized  $g_{21}^2$ ) although they belong to entirely different classes. At the same time,  $G_2^2$  shows different gating patterns to image 1a and image 1b although they are both hummingbirds. However,  $G_2^6$ , lying within a deeper layer of the network, shows similar gating patterns to the two hummingbird images (maximized  $g_{21}^6$ ) while the gating pattern for the electric eel is significantly different. To further understand the basis of this behaviour, we next explore which features maximize each gate.

## 7.2. What Maximizes Gates?

To understand the type of features (context) which maximizes a particular gate and, hence, to further describe the aforementioned gating patterns, we plot the images in the validation set which maximally and minimally activate a particular gating neuron. Also, we freeze the trained network and synthesize the network input, such that the particular gating neuron (before softmax activation) is maximized. This is similar to the gradient ascent process introduced in Simonyan *et al.* 2015 [24]. We choose four gating vectors to  $G_2^2$ ,  $G_1^6$ ,  $G_2^6$  and  $G_1^7$  for this visualization where the vectors  $G_2^2$  and  $G_2^6$  are the gate vectors we discussed in the previous visualization. Since among a gating pair, one gating neuron is inversely related to the other gating neuron due to the softmax activation, maximizing one gate results in minimizing the other. Therefore we choose only one gating neuron from each pair for visualization—gating neurons  $g_{21}^2$ ,  $g_{11}^6$ ,  $g_{21}^6$  and  $g_{11}^7$  from each gating vector respectively.

Figure 9 shows the output of this visualization. In each subfigure, the 10 images which give the maximum gate activation are plotted in the top left and the 10 images which give the minimum activation are plotted in

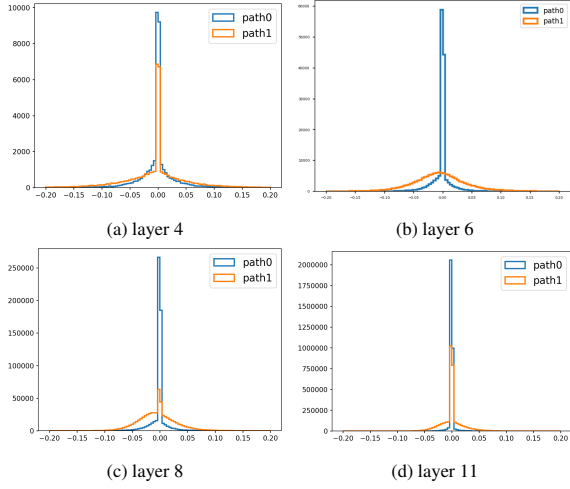


Figure 11: Weights histograms of parallel convolutional or dense operations at selected layers. Each sub-figure denotes the weight histograms of two parallel operations in the corresponding layer. Differences in histograms in the same layer show that parallel paths have learned different portions of information.

the bottom left. Towards the right, the synthesized image such that the gate neuron is maximized is shown. Gate  $g_{21}^2$  (Fig 9a), within initial layers, is maximized for overall colour of blue which is fairly a low-level detail. However, all other gates which are within the deeper layers get maximized for rather complex patterns.  $g_{11}^6$  gets maximized for body patterns of snakes,  $g_{21}^6$  is maximized with bird poses and patterns and  $g_{11}^7$  is triggered best by animal poses with the raised thorax. In each case, the synthesized image shows patterns which maximized the corresponding gate, and that they agree on the top 10 activated images.

Based on the maximization patterns of  $g_{21}^2$  and  $g_{21}^6$ , we can interpret the gating behaviour in the routing visualizations shown in Section 7.1.  $g_{21}^2$  is maximally activated for blue, therefore, with the backgrounds highly composed of blue, activation for image 1b and image 1c get  $g_{21}^2$  maximized, while image 1a, although belongs to the same class as image 1b, shows a lower  $g_{21}^2$  activation.  $g_{21}^6$ , within deeper layers, gets maximized for bird poses and patterns. The two hummingbird images (image 1a and image 1b maximize this gate while the electric eel (image 1c) shows a lower activation. This behaviour highlights that the image context which is related to the task is distributed along with the depth of the trained network. Since resource allocation in different stages of depth is, therefore, different from each other, depending on the level of context represented in that depth, it is important to have routing layers within

the network per segment of layers.

### 7.3. Class-Wise Gating Patterns

The resource allocation in each layer of our multi-path networks depends on the nature of the feature maps in that particular depth. To investigate on any influence of the class to gating patterns, we plot the gate response of selected classes for the gates  $g_{21}^2$  and  $g_{21}^6$ . We choose four classes for this purpose, namely, white shark, sea snake, scorpion, and hummingbird, and record the gate response for all images belonging to each class in the ILSVRC 2012 validation set. Figure 10 summarizes the gate activation histograms for these 4 classes.

Class white shark, having blue sea water as dominant detail in most cases, show overall high activation for  $g_{21}^2$ . The other classes show even distribution of  $g_{21}^2$  since those classes contain instances which may or may not contain dominant blue. Also, class hummingbird, with bird poses and patterns show overall high activation for  $g_{21}^6$ , which triggers for bird patterns. The other classes, however, show overall less  $g_{21}^6$  activations since they hardly agree on bird patterns. This reveals that the image context which matters to the gating—hence, resource allocation in each layer—is a complex detail which expands beyond just the class. However, due to the unique nature of certain classes, most of their members may show similar gating patterns in certain layers. This happens when the triggering pattern for the particular gate is mostly a part of the class members.

### 7.4. Weights of Parallel Computations

One of the reasons for introducing multi-path networks with routing schemes is to group homogeneous feature maps to parallel paths and let the parallel filter sets of the same layer to learn different portions of information. With this, during inference, relevant features can be extracted using the data-dependent routing mechanism. To ensure that our approach has successfully enabled this, we plot the weights histograms of the VGG13-2 selected layers which carry two parallel convolutions or dense operations on the two sets of feature maps, which are independent of each other. Figure 11 shows the weights histograms of the two parallel operations at layer 4, 6, 8 and 11. Layer 11 is a dense layer while the other layers are convolutional. The histograms of parallel paths being distinct confirm that the parallel paths have learned different portions of information.

## 8. Conclusion

The resource consumption of training and modeling deep networks are mostly overwhelming. Thus, it is



important to design a network with perfect harmony in depth and width to effectively utilize every trainable parameter. In this paper, we explored ways to strengthen layer-wise feature extraction by implementing parallel paths. In particular, instead of naive network widening, we presented stacking parallel paths into a single network and using novel mechanisms to intelligently route among parallel paths end-to-end in a data-dependent manner. Our multi-path networks consistently achieved improved classification accuracy compared to existing widening techniques with similar complexity. Ours also displayed superior performance to existing adaptive learning strategies. Our networks even attained slightly better results than thin deeper networks with similar or more number of parameters. We empirically validated the nature of input dependency of the proposed routing mechanisms and the ability to extract distinct features in parallel paths. The ability of our multi-path networks to take slightly different path combinations according to the context of the input is impressive and can be interpreted as an adaptive single model, that softly switches between different sub-modules. Furthermore, it would be intuitive to expand the soft routing towards discrete routing to increase the capacity of the multi-path networks to cater for even multiple datasets at once.

## References

- [1] Caruana, R., 1997. Multitask learning. *Machine learning* 28, 41–75.
- [2] Ciregan, D., Meier, U., Schmidhuber, J., 2012. Multi-column deep neural networks for image classification, in: *Proceedings of the IEEE Conference on Computer Vision and Pattern Recognition (CVPR)*, pp. 3642–3649.
- [3] Deng, J., Dong, W., Socher, R., Li, L.J., Li, K., Fei-Fei, L., 2009. Imagenet: A large-scale hierarchical image database, in: *2009 IEEE conference on computer vision and pattern recognition*, Ieee. pp. 248–255.
- [4] Facebook, . fb.resnet.torch. URL: <https://github.com/facebookarchive/fb.resnet.torch>.
- [5] Gao, Y., Ma, J., Zhao, M., Liu, W., Yuille, A.L., 2019. Nddr-cnn: Layerwise feature fusing in multi-task cnns by neural discriminative dimensionality reduction, in: *Proceedings of the IEEE Conference on Computer Vision and Pattern Recognition (CVPR)*, pp. 3205–3214.
- [6] Glorot, X., Bordes, A., Bengio, Y., 2011. Deep sparse rectifier neural networks, in: *Proceedings of the fourteenth international conference on artificial intelligence and statistics*, pp. 315–323.
- [7] Ha, D., Dai, A., Le, Q.V., 2016. Hypernetworks. *arXiv preprint arXiv:1609.09106*.
- [8] Ha, D., Dai, A., Le, Q.V., 2017. Hypernetworks, in: *Proceedings of International Conference on Learning Representations (ICLR)*.
- [9] He, K., Zhang, X., Ren, S., Sun, J., 2016a. Deep residual learning for image recognition, in: *Proceedings of the IEEE Conference on Computer Vision and Pattern Recognition (CVPR)*, pp. 770–778.
- [10] He, K., Zhang, X., Ren, S., Sun, J., 2016b. Identity mappings in deep residual networks, in: *European Conference on Computer Vision (ECCV)*, Springer. pp. 630–645.
- [11] Hinton, G.E., Sabour, S., Frosst, N., 2018. Matrix capsules with EM routing, in: *Proceedings of International Conference on Learning Representations (ICLR)*.
- [12] Hu, J., Shen, L., Albanie, S., Sun, G., Vedaldi, A., 2018a. Gather-excite: Exploiting feature context in convolutional neural networks, in: *Advances in Neural Information Processing Systems*, pp. 9401–9411.
- [13] Hu, J., Shen, L., Sun, G., 2018b. Squeeze-and-excitation networks, in: *Proceedings of the IEEE Conference on Computer Vision and Pattern Recognition (CVPR)*, pp. 7132–7141.
- [14] Kahatapitiya, K., Tissera, D., Rodrigo, R., 2019. Context-aware automatic occlusion removal, in: *2019 IEEE International Conference on Image Processing (ICIP)*, IEEE. pp. 1895–1899.
- [15] Krizhevsky, A., Hinton, G., et al., 2009. Learning multiple layers of features from tiny images. Technical Report. Citeseer.
- [16] Krizhevsky, A., Sutskever, I., Hinton, G.E., 2012. Imagenet classification with deep convolutional neural networks, in: *Advances in Neural Information Processing Systems*, pp. 1097–1105.
- [17] LeCun, Y., Bottou, L., Bengio, Y., Haffner, P., 1998. Gradient-based learning applied to document recognition. *Proceedings of the IEEE* 86, 2278–2324.
- [18] Misra, I., Shrivastava, A., Gupta, A., Hebert, M., 2016. Cross-stitch networks for multi-task learning, in: *Proceedings of the IEEE Conference on Computer Vision and Pattern Recognition (CVPR)*, pp. 3994–4003.
- [19] Romero, A., Ballas, N., Kahou, S.E., Chassang, A., Gatta, C., Bengio, Y., 2015. Fitnets: Hints for thin deep nets, in: *Proceedings of International Conference on Learning Representations (ICLR)*.
- [20] Ruder, S., Bingel, J., Augenstein, I., Søgaard, A., 2019. Latent multi-task architecture learning, in: *Proceedings of AAAI Conference of Artificial Intelligence*, pp. 4822–4829.
- [21] Rumelhart, D.E., Hinton, G.E., Williams, R.J., 1986. Learning representations by back-propagating errors. *Nature* 323, 533.
- [22] Russakovsky, O., Deng, J., Su, H., Krause, J., Satheesh, S., Ma, S., Huang, Z., Karpathy, A., Khosla, A., Bernstein, M., Berg, A.C., Fei-Fei, L., 2015. ImageNet Large Scale Visual Recognition Challenge. *International Journal of Computer Vision (IJCV)* 115, 211–252. doi:10.1007/s11263-015-0816-y.
- [23] Sabour, S., Frosst, N., Hinton, G.E., 2017. Dynamic routing between capsules, in: *Advances in Neural Information Processing Systems*, pp. 3856–3866.
- [24] Simonyan, K., Vedaldi, A., Zisserman, A., 2013. Deep inside convolutional networks: Visualising image classification models and saliency maps. *arXiv preprint arXiv:1312.6034*.
- [25] Simonyan, K., Zisserman, A., 2014. Very deep convolutional networks for large-scale image recognition. *arXiv preprint arXiv:1409.1556*.
- [26] Srivastava, R.K., Greff, K., Schmidhuber, J., 2015a. Highway networks. *arXiv preprint arXiv:1505.00387*.
- [27] Srivastava, R.K., Greff, K., Schmidhuber, J., 2015b. Training very deep networks, in: *Advances in neural information processing systems*, pp. 2377–2385.
- [28] Szegedy, C., Ioffe, S., Vanhoucke, V., Alemi, A.A., 2017. Inception-v4, inception-resnet and the impact of residual connections on learning, in: *AAAI Conference on Artificial Intelligence*.
- [29] Szegedy, C., Liu, W., Jia, Y., Sermanet, P., Reed, S., Anguelov, D., Erhan, D., Vanhoucke, V., Rabinovich, A., 2015. Going deeper with convolutions, in: *Proceedings of the IEEE Conference on Computer Vision and Pattern Recognition (CVPR)*, pp. 1–9.



- [30] Szegedy, C., Vanhoucke, V., Ioffe, S., Shlens, J., Wojna, Z., 2016. Rethinking the inception architecture for computer vision, in: Proceedings of the IEEE conference on computer vision and pattern recognition, pp. 2818–2826.
- [31] Tissera, D., Vithanae, K., Wijesinghe, R., Kahatapitiya, K., Fernando, S., Rodrigo, R., 2020. Feature-dependant cross-connections in multi-path neural networks, in: International Conference on Pattern Recognition (ICPR), IAPR.
- [32] Veit, A., Belongie, S., 2018. Convolutional networks with adaptive inference graphs, in: European Conference on Computer Vision, pp. 3–18.
- [33] Wang, M., 2015. Multi-path convolutional neural networks for complex image classification. arXiv preprint arXiv:1506.04701 .
- [34] Wang, Q., Wu, B., Zhu, P., Li, P., Zuo, W., Hu, Q., 2019. Eca-net: Efficient channel attention for deep convolutional neural networks. arXiv preprint arXiv:1910.03151 .
- [35] Wu, Z., Nagarajan, T., Kumar, A., Rennie, S., Davis, L.S., Grauman, K., Feris, R., 2018. Blockdrop: Dynamic inference paths in residual networks, in: Proceedings of the IEEE Conference on Computer Vision and Pattern Recognition (CVPR), pp. 8817–8826.
- [36] Xie, S., Girshick, R., Dollár, P., Tu, Z., He, K., 2017. Aggregated residual transformations for deep neural networks, in: Proceedings of the IEEE Conference on Computer Vision and Pattern Recognition (CVPR), pp. 1492–1500.
- [37] Zagoruyko, S., Komodakis, N., 2016. Wide residual networks, in: Proceedings of the British Machine Vision Conference (BMVC), pp. 87.1–87.12.